SCIENCE CHINA
Life Sciences

•RESEARCH PAPER•

May 2019 Vol.62 No.5: 668–680
https://doi.org/10.1007/s11427-018-9369-3

Cyclin Cyc2p is required for micronuclear bouquet formation in *Tetrahymena thermophila*

Jing Xu[1,2,3], Xiaoxiong Li[3], Weibo Song[1,4], Wei Wang[3*] & Shan Gao[1,4,5*]

[1]*Institute of Evolution & Marine Biodiversity, Ocean University of China, Qingdao 266003, China;*
[2]*College of Life Science, Shanxi University, Taiyuan 030006, China;*
[3]*Key Laboratory of Chemical Biology and Molecular Engineering of the Ministry of Education, Institute of Biotechnology, Shanxi University, Taiyuan 030006, China;*
[4]*Laboratory for Marine Biology and Biotechnology, Qingdao National Laboratory for Marine Science and Technology, Qingdao 266003, China;*
[5]*College of Marine Life Sciences, Ocean University of China, Qingdao 266003, China*

Received September 18, 2018; accepted November 19, 2018; published online February 27, 2019

Meiotic bouquet formation (known as crescent formation in *Tetrahymena thermophila*) is indispensable for homologous pairing and recombination, but the regulatory mechanism of bouquet formation remains largely unknown. As a conjugation specific cyclin gene, *CYC2* knockout mutants failed to form an elongated crescent structure and aborted meiosis progress in *T. thermophila*. γ-H2A.X staining revealed fewer micronuclear DNA double-strand breaks (DSBs) in *cyc2*Δ cells than in wild-type cells. Furthermore, *cyc2*Δ cells still failed to form a crescent structure even though DSBs were induced by exogenous agents, indicating that a lack of DSBs was not completely responsible for failure to enter the crescent stage. Tubulin staining showed that impaired perinuclear microtubule structure may contribute to the blockage in micronuclear elongation. At the same time, expression of microtubule-associated kinesin genes, *KIN11* and *KIN141*, was significantly downregulated in *cyc2*Δ cells. Moreover, micronuclear specific accumulation of heterochromatin marker trimethylated H3K23 abnormally increased in the *cyc2*Δ mutants. Together, these results show that cyclin Cyc2p is required for micronuclear bouquet formation via controlling microtubule-directed nuclear elongation in *Tetrahymena*.

***Tetrahymena*, meiosis, cyclin Cyc2p, bouquet formation**

Citation: Xu, J., Li, X., Song, W., Wang, W., and Gao, S. (2019). Cyclin Cyc2p is required for micronuclear bouquet formation in *Tetrahymena thermophila*. Sci China Life Sci 62, 668–680. https://doi.org/10.1007/s11427-018-9369-3

INTRODUCTION

Meiosis occurs in all sexually reproducing unicellular and multicellular eukaryotes. During leptotene-zygotene of meiosis I stage, telomeres cluster into a small area at the nuclear periphery and nuclei become stretched to form the chromosomal bouquet (Carlton et al., 2003; Golczyk et al., 2008; Trelles-Sticken et al., 1999). The bouquet is an evolutionarily conserved structure that occurs in most eukaryotic organisms and is essential for homologous chromosome alignment and pairing (Zickler and Kleckner, 2016). Previous studies identified several key proteins required for bouquet formation; one of them is cyclin-dependent kinases (CDKs) and their regulatory cyclin subunits, which are indispensable for controlling meiotic progression at multiple checkpoints (Morgan, 1997). Murine cyclin A1 is essential for entry into metaphase of meiosis I during spermatogenesis (Müller-Tidow et al., 2004), and loss of the *Arabidopsis* A1-type cyclin results in delayed cell cycle progression at pa-

*Corresponding authors (Wei Wang, Email: gene@sxu.edu.cn; Shan Gao, email: shangao@ouc.edu.cn)

chytene and meiosis II (Magnard et al., 2001). Cyclin B2 phosphorylation promotes oocyte development in *Xenopus* (Gautier and Maller, 1991). Zebrafish cyclin B3 localizes to the perinuclear region in large germ-cell cysts (Ozaki et al., 2011), murine cyclin B3 controls the onset of meiosis anaphase in oocytes (Zhang et al., 2015), and mammalian cyclin B3 facilitates synaptonemal complex formation and prevents precocious pachytene entry during spermatogenesis (Nguyen et al., 2002; Tschöp et al., 2006).

Tetrahymena thermophila is a unicellular ciliated protist that has been widely used as a model organism in cell biology as well as in genetics and epigenetics (Chen et al., 2016; Collins and Gorovsky, 2005; Gao et al., 2013; Wang et al., 2017; Wang et al., 2017; Zhao et al., 2017). During vegetative growth, the polyploid somatic macronucleus (Mac) is transcriptionally active, whereas the diploid micronucleus (Mic) is transcriptionally silent (Orias et al., 2011; Wang Y R et al., 2017). Mic meiosis is induced when starved cells of two different mating types are mixed together (Wolfe, 1973). Mic morphology changes dramatically throughout meiotic prophase I and has been classified into six distinct stages (Loidl and Mochizuki, 2009; Martindale et al., 1982): stage I, spherical; early stage II, drop or egg shape; late stage II, spindle shape; stage III, torch shape; stage IV, thread-like crescent; and stages V and VI, progressive shortening Mic (Figure 1). The *Tetrahymena* Mic crescent structure is functionally equivalent to the general meiotic bouquet structure. It is formed when the Mic becomes maximally stretched (by about 50-fold) during leptotene–zygotene transition in the first meiotic prophase (Orias et al., 2011). Homologous chromosome pairing occurs during Mic elongation, while telomeres and centromeres are pushed to opposite poles (Loidl and Mochizuki, 2009; Loidl and Scherthan, 2004). 34 cyclin homologs were identified in *Tetrahymena* (*Tetrahymena* Genome Database (TGD); http://www.ciliate.org), however, their function was less investigated (Stover et al., 2006; Yan et al., 2016b). *CYC2*, *CYC17*, and *CYC28* were conjugation specific expressed genes. Cyc17 is essential for anaphase initiation and chromosome segregation (Yan et al., 2016a) and Cyc2p plays a key role during meiosis (Xu et al., 2016). Similarly, the cyclin-dependent kinase Cdk3 is also involved in initiating meiosis (Yan et al., 2016b). Functional analysis of the specific *Tetrahymena* cyclins is important for understanding molecular mechanism of bouquet formation.

In the present study, we performed a detailed investigation of Cyc2p function and its regulation mechanism during micronuclear elongation. *cyc2*Δ cells fail to form crescent structure and arrest in early prophase of meiosis I. The microtubule structure involved in nuclear envelope is abnormal and expression of two kinesin genes significantly down-regulated in *cyc2*Δ cells. Cyc2p regulates both micronuclear DSB formation and micronuclear microtubule dynamics. These results indicate that cyclin Cyc2p is required for micronuclear meiosis via controlling microtubule-directed nuclear elongation in *Tetrahymena* meiotic prophase.

RESULTS

Characterization of *Tetrahymena* Cyc2p

CYC2 has conjugation-specific expression (http://tfgd.ihb.ac.cn) (Xiong et al., 2013). We found that *CYC2* is not expressed during vegetative growth and starvation, but is dra-

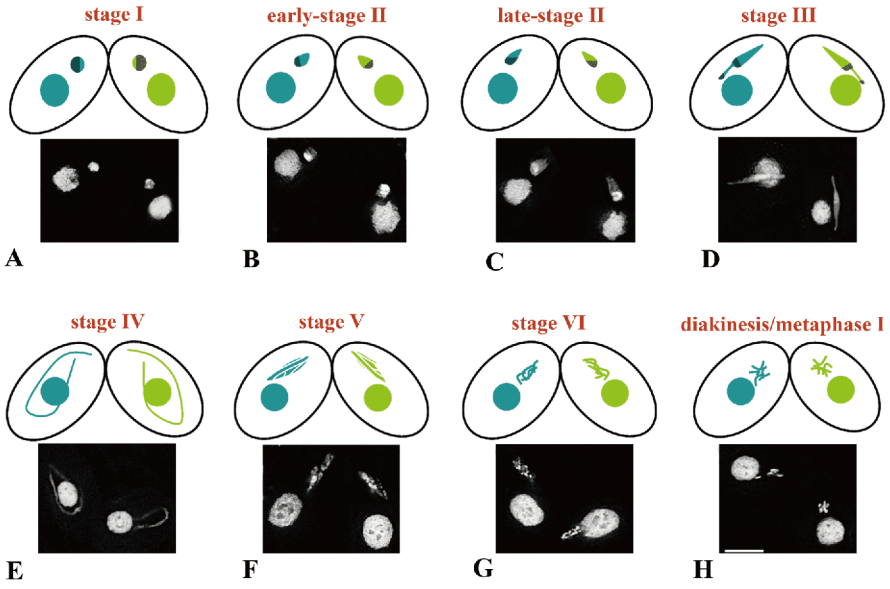

Figure 1 Development of the meiotic Mic in *Tetrahymena*. Schematic diagram showing Mic development during meiotic prophase I (A–H), as indicated by DAPI staining (A–H). Stages are classified according to Sugai and Hiwatashi, (1974) and Loidl and Scherthan, (2004).

matically induced soon after meiosis initiation (Figure S1A in Supporting Information). The *CYC2* gene is 2126 bp, with an open reading frame of 1839 bp, and encodes a 612 amino acid protein, Cyc2p (Figure S1B) containing a cytoplasmic retention signal (at amino acids 26–95), a rich-lysine motif (at amino acids 157–197), a typical destruction box (RXXLXXIXN, at amino acids 269–277), and a conserved cyclin box region (at amino acids 373–467). A candidate phosphorylation site (SPQK; at amino acids 311–314) for mediating ubiquitin-dependent degradation was identified (Yan et al., 2016b).

To determine Cyc2p localization, two hemagglutinin (HA) tags were added to the C-terminus of the endogenous *CYC2* gene (Figure S1C). Immunofluorescence staining showed that Cyc2p-HA was mainly distributed throughout the cytoplasm during conjugation (Figure S1D). To more clearly monitor Cyc2p distribution, *CYC2* over-expressing construct was created. Two hemagglutinin (HA) tags were added to the N-terminus of *CYC2* (Figure 2A). *CYC2* over-expressing mutants were generated (OE-*CYC2*-B and OE-*CYC2*-C) by replacing the *MTT1* gene (Figure S2A). Overexpressed Cyc2p was localized in the cytoplasm throughout conjugation and also to the Mic at all meiotic stages (Figure 2B, a–d).

The cyclin B1 cytoplasmic retention signal (CRS) is sufficient to restrict protein localization to the cytoplasm in human cells (Pines and Hunter, 1994). To explore the function of the CRS in Cyc2p, we constructed a truncated HA-tagged *CYC2* mutant to express CRS-Cyc2p lacking the N-terminal 131 amino acids (including the CRS; Figure 2C and S2B, C. The truncated Cyc2p preferentially localized to the Mic during meiotic prophase I (Figure 2D). Cyclin B was previously reported to shuttle between the nucleus and cytoplasm; this protein can be specifically exported from the nucleus, leading to mainly cytoplasmic localization (Hagting et al., 1998; Lindqvist et al., 2009; Pines and Hunter, 1994). In the present study, Cyc2p underwent relocalization to Mics following overexpression of the full-length protein or deletion of the CRS. Therefore, we speculate that Cyc2p undergoes micronuclear–cytoplasmic shuttling in *Tetrahymena*.

Cyc2p is required for micronuclear crescent formation

CYC2 knockout strains were obtained using the co-Deletion method (Hayashi and Mochizuki, 2015). We also generated *cyc2*Δ cells of two mating types (B2086 and CU428) by introducing the knockout construct into the parental macronucleus using a biolistic particle delivery system (Figure 3A)

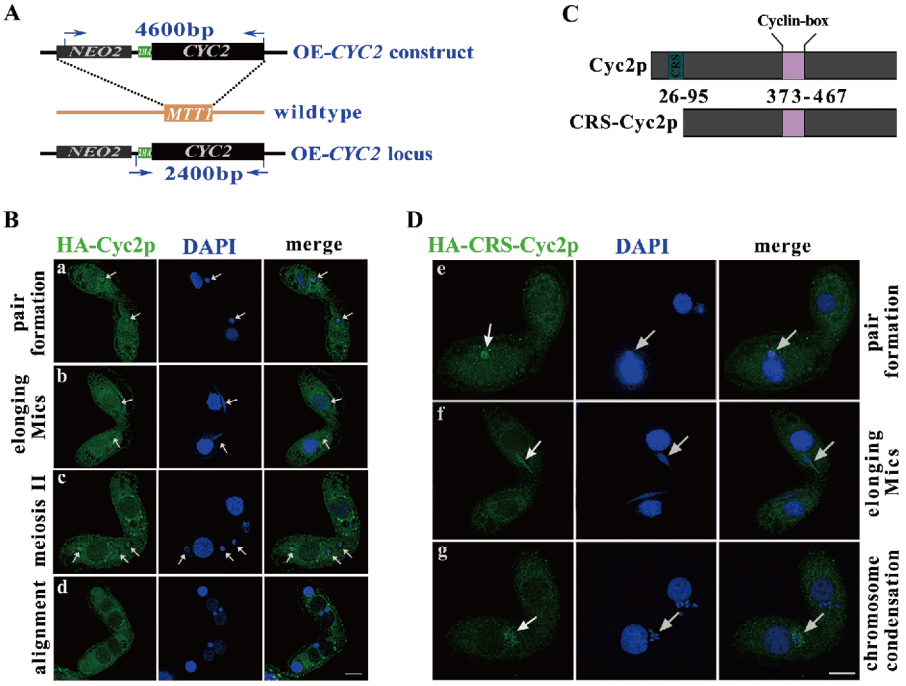

Figure 2 Localization of Cyc2p and truncated Cyc2p. A, Schematic diagram showing OE-HA-*CYC2* construction. Two tandem HA coding sequences were inserted before *CYC2*. The NEO2 cassette confers resistance to paromomycin. B, Localization of HA-Cyc2p. Cells expressing OE-*CYC2*-B were mixed with those expressing OE-*CYC2*-C and mating cells were collected after 2, 4, 6, 8, 10, 12, 14, and 24 h. Cell samples were analyzed by immunofluorescence staining using anti-HA primary antibody and FITC-conjugated secondary antibody. DNA was stained with DAPI (Xu et al., 2012). a, Pair formation, b, elongating Mics, c, meiosis II, and (d) nuclear alignment. Arrows indicate Mics. Scale bar, 10 μm. C, Schematic diagram of Cyc2p and CRS-Cyc2p proteins. Numbers indicate the amino acid position for each domain. D, Localization of truncated CRS-Cyc2p. A strain harboring CRS-CYC2-B was mated with the WT strain. Mating cells were collected at 2 and 3 h after mixing and analyzed by immunofluorescence staining with anti-HA primary antibody and FITC-conjugated secondary antibody. DNA was stained with DAPI. e, Pair formation, f, elongating Mics, and (g) chromosome condensation. Arrows indicate Mics. Scale bar, 10 μm.

(Cassidy-Hanley et al., 1997). The *CYC2* knockout strains, *cyc2*Δ-B and *cyc2*Δ-C, were obtained by phenotypic assortment. Complete deletion of *CYC2* from the somatic genome (Figure 3B) (Hayashi and Mochizuki, 2015; Orias and Flacks, 1975) was confirmed by the lack of detectable *CYC2* transcripts at all tested conjugation stages in mating *cyc2*Δ cells (Figure 3C).

Vegetatively growing *cyc2*Δ cells proliferated normally, consistent with *CYC2* characterization as a conjugation-specific gene (Figure S1A). The phenotype of *cyc2*Δ cells during conjugation was as previously reported (Xu et al., 2016): cells initiated mating at 2 h after mixing (Figure 3D, d), but micronuclear elongation was arrested at prophase stage II (spindle-shaped Mic; Figure 3D, f). Subsequently, the developing Mics lost polarity and fully retracted to form spheres (Figure 3D, j, k). At 5 h after mixing, ~90% of Mics had returned to prophase stage I (spherical; Figure 3F) and only ~10% were still at stage II (spindle shape; Figure 3F). Mating the *cyc2*Δ mutant with wild-type (WT) cells was sufficient to rescue the abnormal phenotype. These results indicate that Cyc2p is required for Mic elongation.

In WT cells, γ-H2A.X signal was observed in prophase mid-stage II (Figure 4A, c) and became stronger as cells progressed tolate stage II (Figure 4A, d). In *cyc2*Δ cells, the γ-H2A.X signal was transiently seen at early stage II (drop- or egg-shaped Mic; Figure 4A, f) but had disappeared by mid-stage II (Figure 4A, g, h). Interestingly, the mRNA expression of *RAD51* (essential for meiotic DSB repair) (Howard-Till et al., 2011) and *DMC1* (promotes strand exchange during homologous recombination) (Howard-Till et al., 2011) increased slightly (by 1.3-fold and 1.5-fold, respectively) at 2 h after mixing (Figure 4C). It is tempting to speculate that the consequent slight increase in Rad51p and Dmc1p levels could be necessary to repair transient DSBs in early stage II (Figure 4A, f), although we cannot explain why DSBs should be formed at this stage.

DSB deficiency and Mic elongation arrest were also observed in mating cells lacking the *SPO11* gene (TTHERM_00627090), which encodes a protein that catalyzes DSB formation (Loidl and Mochizuki, 2009; Mochizuki et al., 2008). When DSBs were induced in *spo11*Δ cells by cisplatin (CP) or methyl methanesulfonate (MMS) treatment, the arrested spindle-shaped Mics became fully elongated and γ-H2A.X foci reappeared (Loidl and Mochizuki, 2009; Mochizuki et al., 2008). Consistent with this finding, *SPO11* expression was greatly decreased (by 3171-fold and 628-fold, respectively) in *cyc2*Δ cells at 2 and 3 h after mixing (Figure 4C). This result could explain the absence of DSBs in mid stage II Mics in *cyc2*Δ cells. However, despite DNA lesions or DSB formation (as indicated by γ-H2A.X staining; Figure 4B), Mics in *cyc2*Δ cells treated with CP and MMS still arrested at the spindle-shape stage and failed to develop into a crescent structure. This finding confirms previous speculation that Cyc2p is an upstream regulator of Spo11p (Xu et al., 2016); in this capacity, it might also influence downstream processes other than DSB formation. In a previous study, treatment with CP or ultraviolet radiation failed to restore crescent elongation in cells lacking the *ATR1*

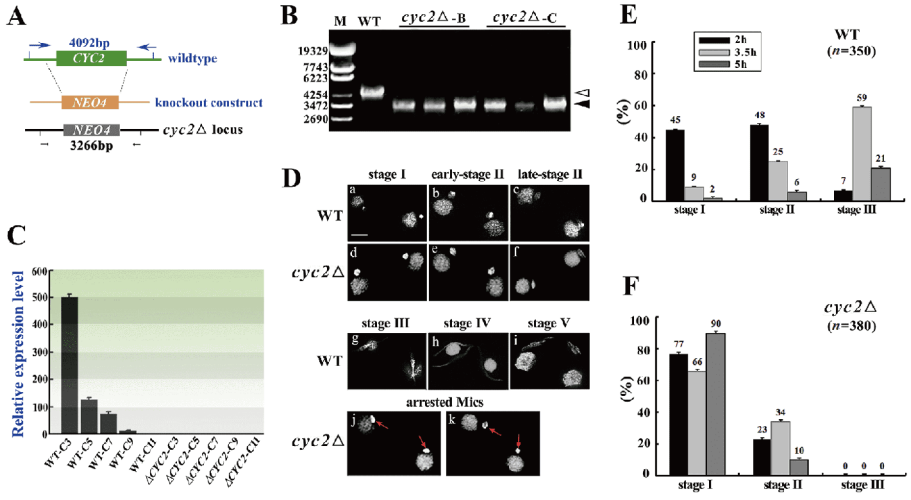

Figure 3 Mic development during prophase I in *CYC2* knockout mutants. A, Schematic diagram showing construction of the *CYC2* knockout. *CYC2* was replaced with a NEO4 cassette in mutant cells. Arrows indicate primer recognition sites. B, *CYC2* knockout mutants Δcyc2-B and Δcyc2-C were confirmed by PCR. White triangle, WT sequence; black triangle, mutant sequence. C, Analysis of *CYC2* expression level: *y*-axis, fold change in relative *CYC2* expression; *x*-axis, conjugation stage (hours after mixing). Total RNA was isolated at 3, 5, 7, 9, and 11 h after mixing. 17S rRNA was used as the internal reference gene. D, Microscopic analysis of changes in Mic structure during meiosis: (a, d) spherical, not compact (stage I); (b, c, e, f) change from egg shaped (early stage II) to spindle shaped (late stage II); (g) changed from spindle shaped to torch shaped (stage III); (h) fully elongated, crescent shaped (stage IV); and (i) start of condensation (stage V). In the cyc2Δ mutant, Mic development was normal until stage II, but progress was arrested after the spindle stage and Mics then retracted to form spheres (j, k). Red arrows indicate arrested Mics. Scale bar, 10 μm. E, F, Development of Mics in WT (E) and cyc2Δ (F) cells. Cells were fixed at 2, 3.5, and 5 h after mixing and stained with DAPI. The number of spherical (stage I), egg-shaped or drop-shaped (stage II), and torch-shaped or fully elongated (crescent stage; stage III) Mics is shown (above bars). Histograms display the mean of three independent biological replicates.

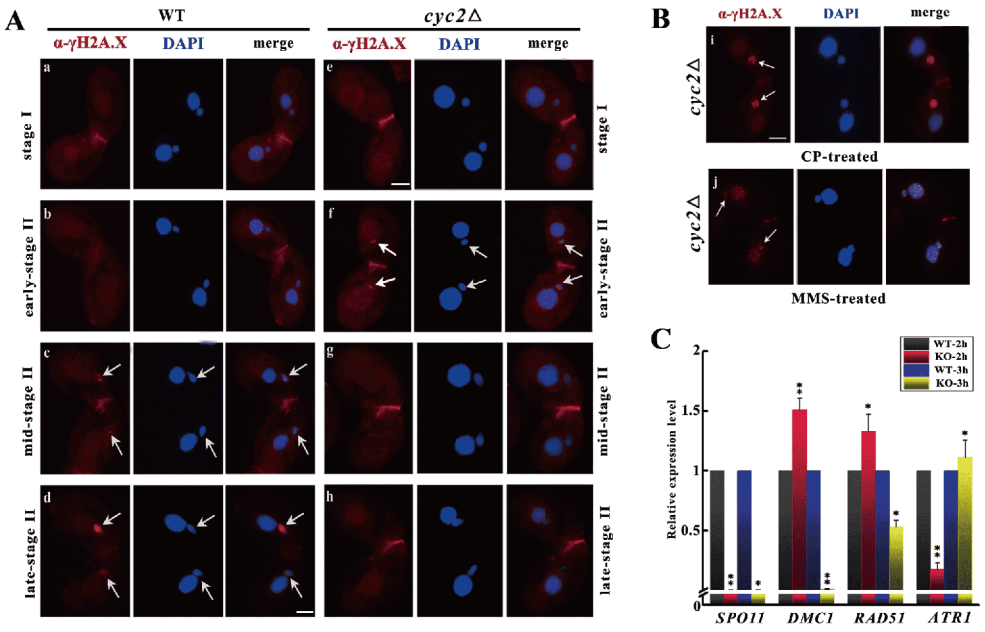

Figure 4 Loss of *CYC2* alters the chromosome breakage pattern during meiotic prophase. A, In WT cells, the γ-H2A.X DSB marker was absent at stage I (a) and early stage II (b), but detectable at mid-stage II (c), increasing in late stage II (d). In the *cyc2*Δ mutant, γ-H2A.X foci were transiently detectable at early stage II (f), but absent in mid-stage II (g) and late stage II (h). Arrows indicate Mics. Scale bar, 10 μm. B, *cyc2*Δ cells fail to form a crescent structure after DSB induction. Mating cyc2Δ cells were treated with CP or MMS and analyzed by γ-H2A.X immunofluorescence. γ-H2A.X signals were restored but Mics still arrested at stage II (spindle shape). Arrows indicate Mics. Scale bar, 10 μm. C, qRT-PCR analysis of relative *SPO11*, *RAD51*, *DMC1* and *ATR1* expression in conjugating cyc2Δ cells at 2 and 3 h after mixing. 17S rRNA was the internal reference gene. WT-2 h and WT-3 h were used as sample references for the respective time points. *, $P<0.05$, **, $P<0.01$.

gene (TTHERM_00108650) (Loidl and Mochizuki, 2009). Interestingly, *ATR1* expression in *cyc2*Δ cells was reduced by 5.8-fold at 2 h after mating (Figure 4C), suggesting that Cyc2p and Atr1p might coregulate an unknown but essential stage(s) of Mic elongation.

Micronuclear centromere clustering is initiated normally in *Cyc2*Δ cells

Telomere and centromere clustering is crucial to form the stretched crescent in *Tetrahymena* (Cui and Gorovsky, 2006; Mochizuki et al., 2008). Centromere clustering occurs prior to the onset of meiosis, followed by its transient dispersal and reassembly within the fully elongated Mics (Loidl and Mochizuki, 2009). To determine whether Cyc2p affects centromere clustering, we assessed the distribution pattern of centromeres by staining with an anti-Cna1p antibody that recognizes the *Tetrahymena* centromeric histone (Cervantes et al., 2006). In WT cells, centromeres were dispersed to the micronuclear periphery during mating pair formation (Figure 5A, a). At the initiation of meiosis, centromeres moved to cluster at a single tip of each Mic (Figure 5A, b, c). This was followed by rearrangement at Mic elongation (Figure 5A, d) and then reassembly into a single focus at the extreme tip of each fully elongated Mic (Figure 5A, e). Centromeres were distributed in *cyc2*Δ cells at stage I (drop-shaped Mic; Figure 5A, f) and clustered at stage II (egg-shaped Mic; Figure 5A, g, h), suggesting that knockout cells initiate centromere clustering. In arrested Mics (that failed to elongate), centromeres became dispersed around the nucleus (Figure 5B, i). The results indicated that internal reorganization of Mics occurred in the *Cyc2*Δmutant, but Mics still failed to elongate.

Micronuclear microtubule structure is altered in *cyc2*Δ cells

Centromeres move in response to pushing forces generated by microtubule bundles emanating from the pole at which telomeres are anchored during meiotic prophase in *Tetrahymena*. Rapid microtubule assembly pushes centromeres to the pole opposite the anchored telomeres, leading to chromosome elongation (Loidl et al., 2012). To explore the role of Cyc2p in this process, we monitored micronuclear microtubule structure by staining with an anti-tubulin antibody. In WT cells, microtubules were distributed around Mic membrane (Figure 6A, a) and gathered together into a focus at the tip of each Mic after chromosome elongation (Figure 6A, b–e). The microtubule structure was similar in WT and *cyc2*Δ cells from stage I to late stage II (Figure 6A, a–c and f–h respectively), but microtubule aggregation was stronger at the chromosome end (thin arrows; Figure 6A, f–h) and the perinuclear region (thick arrows; Figure 6A, h) in *cyc2*Δ cells. After stage II, the intranuclear and perinuclear micro-

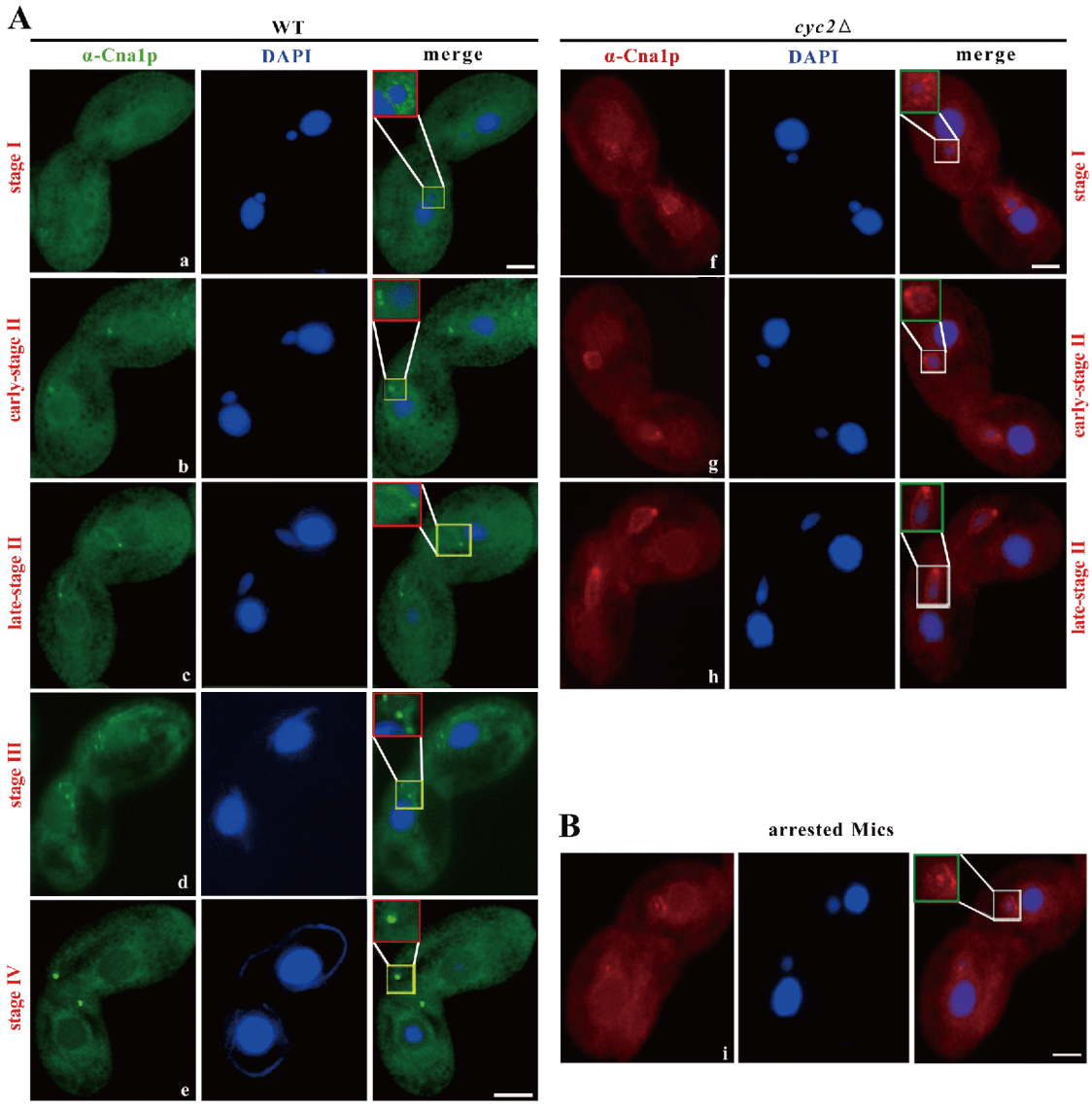

Figure 5 Immunofluorescence staining of the centromeric histone variant Cna1p in WT cells and *cyc2*Δ cells showing centromeres. A, (a) dispersed around the Mic periphery during stage I; (b) grouped together at early stage II (egg- or drop-shaped); (c) aggregated into a point at late stage II; (d) dispersed after Mic elongation; and (e) reassembled into a dot at the tip of fully elongated Mics (stage IV). In the *cyc2*Δ mutant, centromeres were (f) dispersed around Mic periphery in stage I; (g, h) aggregated into a point at late stage II; B, (i) dispersed within retracted Mics. Inset images in the top-left corner of each panel are shown at 4× magnification. Scale bar, 10 μm.

tubule bundles failed to elongate (arrowheads; Figure 6A, i, j). The strongest signal was distributed into the inside of Mics (thin arrows; Figure 6A, i, j). These results indicated that loss of *CYC2* disrupts micronuclear microtubule organization.

The microtubule-associated motor proteins, kinesins, are important for meiotic microtubule dynamics (Camlin et al., 2017). The 14 known kinesin homologs in *Tetrahymena* (Stover et al., 2006; Yan et al., 2016a) were analysed by RNA-seq analysis when samples were collected at 3 h after mixing (Figure 6B). Among them, *KIN11* (TTHERM_00637750) and *KIN141* (TTHERM_00115410) are the most strongly downregulated in *cyc2*Δ mating cells (Stover et al., 2006). We confirmed this by qRT-PCR analysis (Figure 6C): the level of *KIN11* mRNA was reduced by 406-fold and 73-fold, respectively, and the level of *KIN141* mRNA was reduced by 33-fold and 9-fold, respectively, at 2 and 3 h after mixing. We therefore speculate that impaired microtubule movement during early meiosis may be attributable to reduced levels of *KIN11* and *KIN141*.

Trimethylated H3K23 accumulation is increased in *cyc2*Δ cells

Mics are transcriptionally inert during vegetative growth but initiate transcription during meiotic prophase (Martindale et

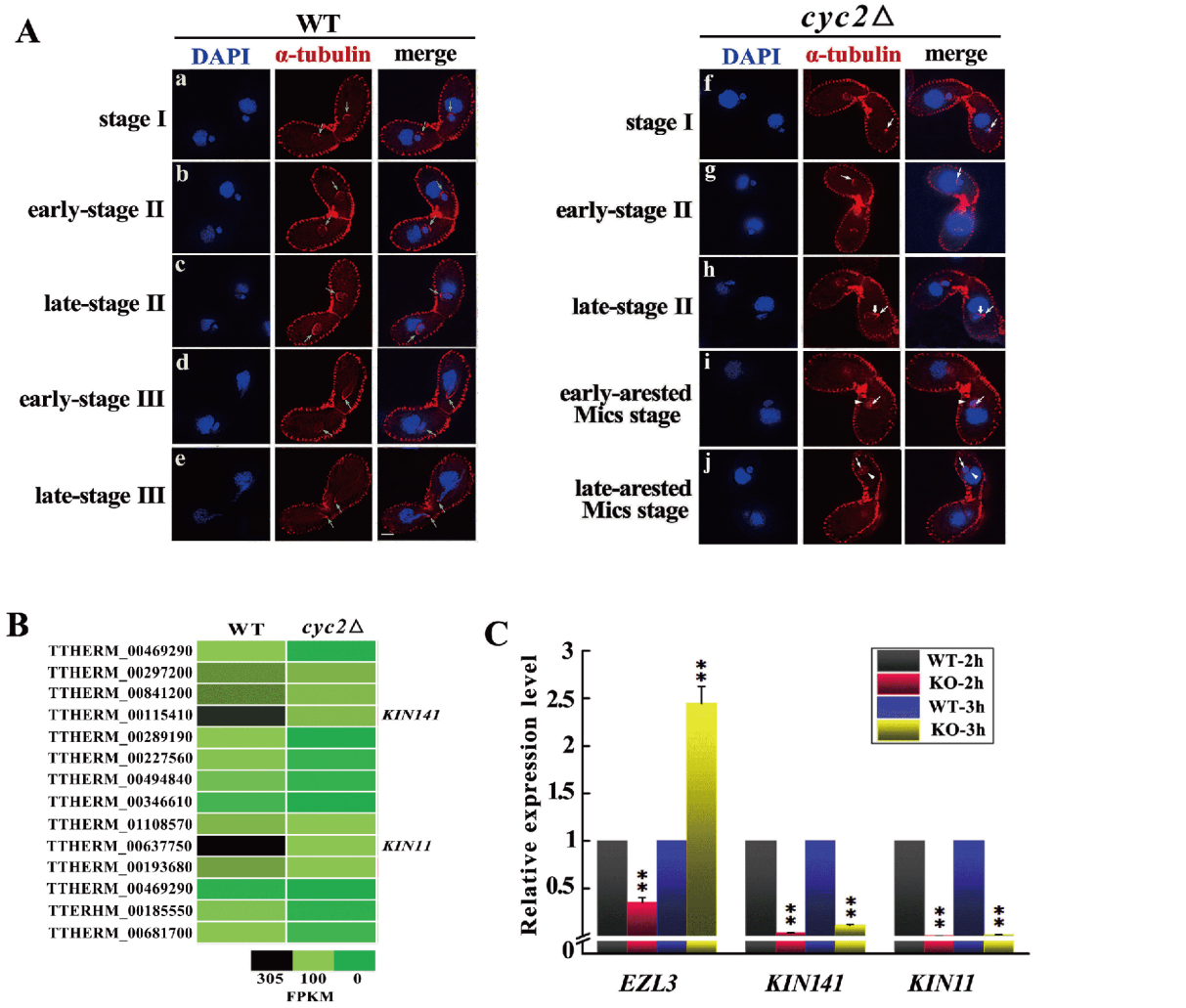

Figure 6 *CYC2* knockout alters micronuclear microtubule organization. A, Localization of α-tubulin in WT and *cyc2*Δ mutant cells. Mating cells were fixed every 0.5 h from 2 h to 3 h after mixing in WT cells or from 2.5 to 6 h after mixing in *cyc2*Δ cells. Microtubule organization in WT cells at (a) stage I, spherical Mic; (b) early stage II, drop-shaped Mic; (c) late stage II, spindle-shaped Mic; (d) early stage III, from spindle-shaped to torch-shaped Mic; and (e) late stage III, torch-shaped Mic. Microtubule organization in *cyc2*Δ cells at (f) stage I, spherical Mic; (g) early stage II, drop-shaped Mic; (h) late stage II, spindle-shaped Mic; (i) early stage of Mic arrest; (j) late stage of Mic arrest. Thin arrows indicate initiation of microtubule bundle; thick arrows indicated the strong perinuclear region; arrowheads indicate retracted nuclear microtubules. Scale bar, 10 μm. B, Heatmap showing differences in the expression of 14 kinesin genes in WT and *cyc2*Δ cells at 3 h after mixing. FPKM values: the highest fold change is 305 and the lowest fold change is 0 (green). C, Expression of *EZL3*, *KIN141*, and *KIN11* mRNA in mating WT and cyc2Δ cells at 2 and 3 h after mixing. 17S rRNA was the internal reference gene. WT-2 h and WT-3 h were used as sample references for the respective time points. *, $P<0.05$, **, $P<0.01$.

al., 1985). The Mic genome is transcribed bi-directionally by RNA polymerase II in meiotic prophase. The resulting double-stranded RNAs are processed to 29 nt scnRNAs by Dcl1p (Noto and Mochizuki, 2017). In *dcl1*Δ cells (in which one of the *Tetrahymena* Dicer homologs is deleted), crescents fail to become fully elongated (Mochizuki and Gorovsky, 2005) and Mic transcripts are not processed into scnRNAs (Woo et al., 2016). To investigate whether Mics are transcriptionally active in *cyc2*Δ cells, scnRNA expression was analyzed. We found that levels of scnRNA expression are comparable in *cyc2*Δ and WT cells (Figure 7A). This result suggests that Mic elongation may not be required for nongenic Mic transcription and scnRNA biogenesis; however, we cannot be sure that the composition of scnRNA pools is the same in WT and *cyc2*Δ cells.

In the absence of the histone methyltransferase Set1, centromere and telomere redistribution are both impaired and bouquet nuclei are absent in *Saccharomyces cerevisiae* (Trelles-Sticken et al., 2005). Trimethylated H3K23 (H3K23me3) is a micronuclear heterochromatin marker in *Tetrahymena* and is enriched at regions proximal to the micronuclear centromere (Papazyan et al., 2014). To further explore whether micronuclear chromatin structure is affected by *cyc2* deletion, we investigated H3K23me3 level in conjugating *cyc2*Δ cells. At 3 h after mixing, H3K23me3 signals were stronger in *cyc2*Δ cells than in WT cells (Figure 7B, Figure S3). Expression of *EZL3* (Papazyan et al., 2014), a gene essential for H3K23me3 deposition in Mics, was also

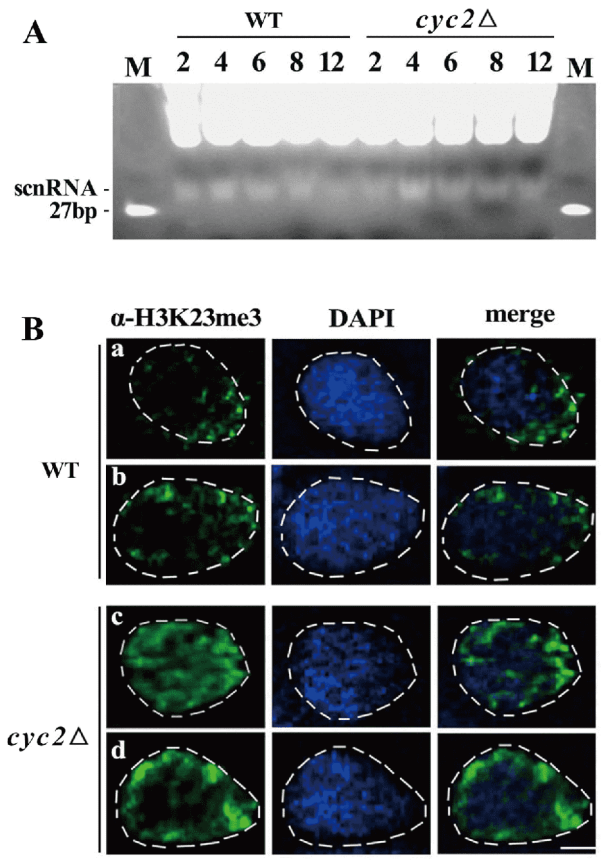

Figure 7 Expression of scnRNAs and localization of H3K23me3 in *cyc2*Δ cells. A, scnRNA expression in mating WT and *cyc2*Δ cells was measured at 2, 4, 6, 8, and 12 h after mixing. RNA isolated from 2×10^6 cells was separated by 12% acrylamide–urea chromatography and stained with ethidium bromide. The 27 nt oligonucleotide was used as a marker. B, Localization of H3K23me3 in Mics at 3 h after mixing. H3K23me3 was distributed in the Mics. H3K23me3 signals were stronger in *cyc2*Δ cells than in WT cells at the early stage II (a, c) and late stage II (b, d) of prophase. Scale bar, 2.5 μm.

increased (by 2.5-fold, relative to WT) at 3 h after mixing in mating *cyc2*Δ cells (Figure 6C). We speculate that increased micronuclear H3K23me3 deposition could affect centromere and telomere redistribution and thereby block Mic elongation in the *cyc2*Δ mutant.

DISCUSSION

Cyc2p could be a member of the conserved cyclin B3 subfamily

Cyclins and CDKs are essential for cell cycle progression (Galderisi et al., 2003). *Tetrahymena* cyclin genes have been classified into three groups based on phylogenetic analyses: canonical cyclins (e.g. A-, B-, D-, and E-type cyclins), transcriptional cyclins (e.g. C-, H-, K-, and Y-type cyclins), and ciliate-specific cyclins (Stover and Rice, 2011). In *Paramecium tetraurelia*, the cyclin family has undergone evolutionary expansion, resulting in 140 homologs (Huysman et al., 2010). In *Tetrahymena*, 34 genes containing a cyclin domain have been identified (Yan et al., 2016a). Expression of almost all of cyclin genes appears to be cell cycle dependent (Stover and Rice, 2011). The number and expression patterns of B-type cyclins vary considerably among organisms, but all contain at least one B1-like and one B3 cyclin gene (Nieduszynski et al., 2002). Chicken cyclin B3 protein was originally identified in interphase cells, where it localizes to the cell nucleus (Gallant and Nigg, 1994). In contrast, mammalian B3 cyclins are specifically expressed in meiotic germ cells; for example, human cyclin B3 is expressed in developing male germ cells and mouse cyclin B3 is expressed at leptotene and zygotene during spermatogenesis (Nguyen et al., 2002).

Previous reports indicate that *CYC2* is a conjugation-specific gene that is highly upregulated at an early stage of conjugation (at 2 h after mixing) (Stover et al., 2006). Consistent with this, we found that *CYC2* deletion blocks meiotic development at the leptotene–zygotene stage. Moreover, BLAST analysis showed that *Tetrahymena* Cyc2p is homologous to *Trichinella* and *Arabidopsis* cyclin B3 (Figure S2D). These results suggest that *Tetrahymena* Cyc2p belongs to the cyclin B3 subfamily.

Only a single cyclin B3 gene has been identified in metazoans (Bourouh et al., 2016); in contrast, the *Tetrahymena* genome encodes a second conjugation-specific cyclin, Cyc17p, that is responsible for separating condensed chromosome during meiosis (Yan et al., 2016a). Cyc17p has high sequence similarity to cyclin B3 proteins in humans, zebrafish, and *Arabidopsis* (Yan et al., 2016a). It is therefore possible that *Tetrahymena* Cyc2p and Cyc17p are both members of the cyclin B3 subfamily.

Mic elongation is regulated by multiple factors

Mic elongation accompanies DSB formation and repair during micronuclear meiosis in *Tetrahymena* (Howard-Till et al., 2011; Mochizuki et al., 2008). In *SPO11* knockout cells (Grelon et al., 2001; Mochizuki et al., 2008), which lack meiotic DSBs and a fully elongated crescent structure, Mic elongation could be restored by treatment with exogenous DNA-damaging agents such as CP and MMS (Loidl and Mochizuki, 2009). Our study demonstrated that loss of *CYC2* drastically decreases both *SPO11* expression and endogenous DSB formation. More importantly, Mic elongation arrest could not be reversed in *cyc2*Δ cells by CP or MMS treatment. These results confirmed that Cyc2p is an upstream regulator of Spo11p (Xu et al., 2016) and that the absence of DSBs is not the only cause of the meiotic defect in *cyc2*Δ cells. It is notable that both *atr1*Δ and *cyc2*Δ cells respond similarly to DNA-damaging reagents (Loidl and Mochizuki, 2009). Moreover, *ATR1* was slightly downregulated at 2 h after mixing, but had returned to WT levels at 3 h after

mixing. These results suggest either that *ATR1* gene expression is only partially dependent on Cyc2p or that Atr1p and Cyc2p regulate meiosis via independent pathways.

Centromeres cluster together and migrate to the DNA-poor Mic tip at the onset of chromosome elongation and the fully elongated stage, but become dispersed at the leading edge of the stretching Mic during intermediate elongation stages (Loidl and Mochizuki, 2009). In the *spo11*Δ mutant, the arrest in centromere rearrangement at the chromosome dispersal stage could be reversed by ultraviolet irradiation (Loidl and Mochizuki, 2009), which also induced to Mic elongation. Consistent with this, caffeine or wortmannin (the kinase inhibitor) treatment prevented both centromere clustering and Mic elongation (Loidl and Mochizuki, 2009), indicating a causal relationship from the former to the latter. However, in *cyc2*Δ mutants, Mics failed to elongate even though centromere clustering was normal at stage II. We therefore speculate that centromere clustering is essential but not sufficient for Mic elongation.

Cyc2p affects chromosome elongation and microtubule structure

When depleting the centromere-specific H3 histone Cna1p, chromosomes do not stretch between the two poles, with a mass of chromatin left behind at one end (Loidl et al., 2012); however, tubulin delineated an elongated chromatin-free extension of Mic (Loidl et al., 2012), revealing an uncoupling of chromosome stretching and Mic extension. Taken together the fact that Mics fail to elongate in the presence of benomyl or nocodazole (microtubule inhibitors) (Loidl and Mochizuki, 2009), we can reason that microtubule structure is essential for Mic elongation. In *cyc2*Δ cells, tubulin failed to elongate in the later stages of prophase I and both chromatin and microtubule bundles retracted at the late crescent stage. In the yeast *S. cerevisiae*, induction of the meiotic cycle leads to a dramatic reorganization of nuclear architecture. Formation of the bouquet depends on the presence of the meiosis-specific telomere protein Ndj1/Tam1 and actin polymerization (Smith et al., 2001; Trelles-Sticken et al., 2005). We therefore reason that the arrested Mic in *cyc2*Δ cells was caused by impaired stretching of microtubule bundles.

Cytoplasmic microtubules and motor proteins bridge the nuclear membranes and are connected to chromatin via a movement-mediating complex (Burke, 2012; Woglar and Jantsch, 2014). Microtubules regulate chromosomes with the aid of motor proteins (Bieling et al., 2010; Niccoli et al., 2004). For example, kinesin-141 is essential for the shrinkage of full crescent microtubules in *Tetrahymena* (Kushida et al., 2017). In *cyc2*Δ cells, *KIN11* and *KIN141* down-regulation was maximal at 3 h after mixing. Therefore, it is plausible that the failure in Mic elongation during early meiosis was partially attributable to reduced levels of *KIN11* and *KIN141*.

In this study, we demonstrated that mating *cyc2*Δ cells fail to form chromatin crescents and arrest at early meiotic prophase I. This defect could be attributed to abnormal microtubule structure and reduced level of kinesin genes. It could also be partially caused by a failure in DSB formation and excessive chromatin aggregation. Based on our results, we conclude that Cyc2p is a key regulator of crescent formation in early meiosis during *Tetrahymena* sexual development.

MATERIALS AND METHODS

Strains and culture

T. thermophila B2086 (mating type II) and CU428 (mating type VII) strains were cultured in SPP medium at 30°C as previously described (Gorovsky et al., 1975). Before mating, cells were starved in 10 mmol L^{-1} Tris-HCl (pH 7.4) without shaking for 18–24 h. Mating was induced by mixing cells of two different mating types together at a final density of 2.5×10^5 cells mL^{-1}.

Plasmid construction

The pNeo4 plasmid (Mochizuki, 2008) and *Neo4* cassette (conferring paromomycin resistance) were used to construct the *CYC2*-HA plasmid to express endogenous levels of hemagglutinin (HA)-tagged Cyc2p in *Tetrahymena*. The 5′ homologous arm of the plasmid comprised a partial coding sequence and an N-terminal 3′ UTR (3′ recombinant homologous arm) sequence of *CYC2*. The two sequences were PCR amplified using the *CYC2*-HA-F1/*CYC2*-HA-R1 and *CYC2*-HA-F2/*CYC2*-HA-R2 primer pairs, respectively, and then connected by overlapping PCR using the *CYC2*–5′-F and *CYC2*–5′-R primers (Table S1 in Supporting Information; *Sac*I and *Not*I restriction sites are underlined). Two HA tags were inserted before the *CYC2* stop codon. The *CYC2* C-terminal 3′ UTR was PCR amplified using the *CYC2*–3′-F and *CYC2*–3′-R primers (Table S1; *Xho*I and *Kpn*I restriction sites are underlined) as the 3′ homologous arm. The 5′ and 3′ homologous arms were digested using *Sac*I/*Not*I and *Xho*I/*Kpn*I, respectively, and cloned into the multiple cloning sites of the pNeo4 vector (digested with the same enzymes).

To create the *CYC2* overexpression plasmid, the complete coding sequence of *CYC2* was PCR amplified using the OE-*CYC2*-F (Table S1; *BamH*I restriction site is underlined) and OE-*CYC2*-R (Table S1; *Asc*I restriction site is underlined) primers. Truncated *CYC2* was PCR amplified using the CRS-*CYC2*-F (Table S1; *BamH*I restriction site is underlined) and OE-*CYC2*-R primers. The amplified sequences were digested with *BamH*I and *Asc*I and cloned into the pXS

vector (digested with the same enzymes).

Expression constructs were introduced into CU428 and B2086 cells by biolistic transformation (Cassidy-Hanley et al., 1997), and paromomycin-resistant transformants were subcloned and cultured in the presence of increasing paromomycin concentrations until cells failed to grow. Completely or partially replaced mutant strains were confirmed by PCR amplification using the *CYC2*-HA-Fjd/*CYC2*-HA-Rjd or OE-Fjd/OE-Rjd primer pairs (Table S1).

Somatic knockout of *CYC2*

The 5′ flanking sequence of *CYC2* was PCR amplified from total genomic DNA was isolated from CU428 using the *CYC2*-KO-5′P1 (Table S1; *Sac*I restriction site is underlined) and *CYC2*-KO-5′P2 (Table S1; *Not*I restriction site is underlined) primers. The 3′ flanking sequence of *CYC2* was PCR amplified from the same template using the *CYC2*-KO-3′P1 (Table S1; *Xho*I restriction site is underlined) and *CYC2*-KO-3P′2 (Table S1; *Kpn*I restriction site is underlined) primers. The *CYC2* 5′- and 3′-flanking sequences were digested with *Sac*I/*Not*I and *Xho*I/*Kpn*I respectively, and cloned into the pNeo4 vector (digested with the same enzymes).

Mutant strains were selected based on paromomycin resistance to obtain complete *CYC2* knockout strains. *CYC2* elimination in the macronucleus was confirmed by PCR amplification using the *CYC2*-KO-Fjd and *CYC2*-KO-Rjd primers (Table S1).

Cytological and immunofluorescence staining

For 4′,6-diamidino-2-phenylindole (DAPI) staining, a 5 mL suspension of conjugating cells was fixed by adding 500 μL 38% formaldehyde and 250 μL 10% Triton X-100 and incubating for 30 min at room temperature (Loidl et al., 2012). Subsequently, cells were sedimented at 1200 r min^{-1} for 1 min and resuspended in 500 μL solution (4% formaldehyde and 3.4% sucrose). The sample was spread onto poly-*L*-lysine-coated slides, washed for 5 min with phosphate-buffered saline (PBS), and incubated with 1 μg mL^{-1} DAPI for 10 min. Slides were treated with 8 μL anti-fading agent.

For HA-Cyc2p immunofluorescence staining, conjugating cells were incubated in Lavdowsky's fixative (ethanol:formalin:acetic acid:water, 50:10:1:39) overnight at 4°C. Cells were then dropped onto coverslips pre-coated with poly-*L*-lysine and air-dried. Coverslips were washed with PBS containing 0.1% Tween-20 (PBST) for 10 min, incubated in blocking solution (PBS containing 10% normal goat serum, 3% BSA, or 0.1% Tween-20) at 30°C for 1 h, and incubated in rabbit anti-HA monoclonal antibody (1:200 dilution; Clone 114–2C-7, Millipore, USA) at 4°C overnight. After washing three times with PBST, coverslips were incubated with FITC-conjugated goat anti-rabbit secondary antibody (1:200 dilution; Millipore, USA) for 1 h at room temperature. Cell samples were then washed in PBST, counterstained with 1 μg mL^{-1} DAPI in PBS, mounted, and visualized by DeltaVision deconvolution fluorescence microscopy (Applied Precision, USA).

For Cna1p, γ-H2A.X, and H3K23me3 immunofluorescence staining, cells were fixed in partial Schaudinn's fixative (saturated $HgCl_2$:ethanol, 2:1) for 5 min at room temperature, washed twice with 5 mL methanol, immobilized on poly-*L*-lysine-coated coverslips, permeabilized, and blocked as described above. For staining, cell samples were incubated for 2 h at room temperature or 30°C with primary antibody: rabbit polyclonal anti-Cna1p antibody (1:200 dilution; kindly provided by Harmit Malik), mouse monoclonal anti-H2A.X phosphorylated (Ser139) antibody (1:200 dilution; Clone 2F3, BioLegend, USA), or rabbit polyclonal anti-histone H3K23me3 antibody (1:200 dilution; 61499, Active Motif, USA). After washing with PBST, samples were incubated with TRITC-conjugated donkey anti-mouse IgG (1:200 dilution; AB10085, Bio Basic, Canada) or FITC/TRITC-conjugated goat anti-rabbit F (ab′) IgG (1:200 dilution; AQ132F, Millipore, USA; AP192R; Millipore, Billerica, MA, USA) for 1 h at room temperature. Cells were washed with PBST, counterstained with 1 μg mL^{-1} DAPI in PBS, mounted, and visualized by DeltaVision deconvolution fluorescence microscopy. The relative fluorescence intensity was analyzed using MetaMorph 7.8.13 software.

For alpha-tubulin immunofluorescence staining, mating cells were fixed with Lavdowsky's fixative and air-dried on coverslips. Cells were permeabilized by washing three times in PBST (10 min each) and then blocked in PBST containing 3% BSA for 1 h. After washing twice in PBST, cells were incubated with anti-α-tubulin mouse monoclonal primary antibody (1:200 dilution; T6074, Sigma, Santa Clara, USA) overnight at 4 °C. After washing five times in PBST, cells were incubated with TRITC-conjugated anti-mouse IgG secondary antibody (1:200 dilution; AB10085, Bio Basic, Canada) for 1 h at room temperature. Cells were washed three times in PBST, counterstained with 1 μg mL^{-1} DAPI in PBS, mounted, and visualized by DeltaVision deconvolution fluorescence microscopy.

qRT-PCR

For each time point, total RNA was extracted from approximately 1×10^6 cells with TRIzol reagent (9010, Takara Biotechnology, Dalian, China). cDNA was synthesized with a random hexamer primer using the PrimerScript™ RT reagent Kit (RR047A, Takara Biotechnology, Dalian, China). Gene expression was measured by qRT-PCR as previously reported, using the primers listed in Table S2, and normal-

ized to 17S rRNA levels.

CP and MMS treatment

CP (6 mg mL^{-1}) and MMS (3.4%) stock solutions were prepared in 10 mmol L^{-1} Tris-HCl buffer. Conjugating cells were treated with 100 μg mL^{-1} CP or 4 mmol L^{-1} (0.034%) MMS at 2 h after mixing and then fixed in partial Schaudinn's fixative at 3.5 h after mixing.

scnRNA analysis

Total RNA was extracted from mating WT and *cyc2*Δ cells. RNA isolated from 2×10^6 cells was resuspended in deionized formamide (F8110, Beijing Solarbio Science & Technology, Beijing, China), separated by 12% polyacrylamide-urea chromatography, and stained with 1.5 μg mL^{-1} ethidium bromide.

Viability assay

At 8–10 h after mixing, individual pairs of conjugating cells were transferred into drops of SPP medium and incubated for 2 d at 30°C. The drops were then transferred into individual wells of 96-well plates and cultured for 24 h. Cell aliquots were transferred to SPP medium containing 15 μg mL^{-1} 6-methylpurine and the remaining cells were transferred to SPP medium containing 100 μg mL^{-1} paromomycin and 1 μg mL^{-1} Cd^{2+}. Only conjugating cells survived in 6-methylpurine; progeny cells were those that failed to grow in paromomycin-containing medium.

RNA-Seq analysis

Approximately 1×10^7 WT cells and *cyc2*Δ mutant cells at 3 h after mixing were flash frozen in 1 mL RNAiso Plus (108-952, Takara Biotechnology) and stored at −80°C. Total RNA was extracted and the purity was assessed using a NanoPhotometer spectrophotometer (Implen, USA). The RNA concentration was measured using a Qubit RNA Assay Kit and Qubit2.0 Fluorometer (Life Technologies, USA) and RNA integrity was assessed using an RNA Nano 6000 Assay Kit and Agilent Bioanalyzer 2100 system (Agilent Technologies, CA, USA). mRNA was purified from total RNA using poly-T oligo-attached magnetic beads (VAHTSTM mRNA-seq V2 Library Prep Kit for Illumina®, NR601-02, Vazyme, Nanjing, China) and used to synthesize cDNA. Library fragments were purified using the AMPure XP system (Beckman Coulter, Beverly, USA) to select cDNA fragments of 80–280 bp in length. PCR was performed using Phusion High-Fidelity DNA polymerase, Universal PCR primers, and the Index (X) Primer. PCR products were purified using the AMPure XP system and library quality was assessed using an Agilent Bioanalyzer 2100 system. Paired-end sequencing was performed using a Hiseq2500PE125 system and raw sequencing reads were trimmed using cutadapt (version 1.2.1) and mapped to the *Tetrahymena thermophila* macronuclear genome assembly (http://ciliate.org/index.php/home/downloads) (Eisen et al., 2006) using TopHat (version 2.1.1) (Ghosh and Chan, 2016). DEGs were removed with Cutdiff software for sequences with less than two-fold changes in FPKM values between WT and *cyc2*Δ. Gene ontology enrichment analysis was carried out with Swiss-Prot (http://web.expasy.org/docs/swiss-prot_guideline.html) and TrEMBL (http://www.bioinfo.pte.hu/more/TrEMBL.htm).

ABBREVIATIONS

Prophase I: prophase of meiosis I; DSBs: DNA double-strand breaks; TGD: *Tetrahymena* Genome Database; scnRNA: scan RNA; Mac: macronucleus; Mic: micronucleus; ATM: the ataxia-telangiectasia mutated; ATR: ATM and RAD3-related; Cdks: cyclin-dependent kinases; CRS: cytoplasmic retention signal; H3K23me3: Trimethylated H3K23; CP: Cisplatin; MMS: Methyl methanesulfonate; PBS: phosphate-buffered saline; DAPI: 4′,6-diamidino-2-phenylindole

AVAILABILITY OF DATA

The latest SB210 MAC genome can be found at the *Tetrahymena* genome database (http://ciliate.org). GEO accession number for publicly available *Tetrahymena* datasets: GSE108064.

Compliance and ethics *The author(s) declare that they have no conflict of interest.*

Acknowledgements *This work was supported by the National Natural Science Foundation of China (31471999, 31572253), Shanxi Scholarship Council of China (200902), Aoshan Science and Technology Innovation Program of the Qingdao National Laboratory for Marine Science and Technology, the China Postdoctoral Science Foundation (2014M551961), and the Natural Science Foundation of Shanxi Province (2015011078).*

References

Bieling, P., Kronja, I., and Surrey, T. (2010). Microtubule motility on reconstituted meiotic chromatin. Curr Biol 20, 763–769.
Bourouh, M., Dhaliwal, R., Rana, K., Sinha, S., Guo, Z., and Swan, A. (2016). Distinct and overlapping requirements for cyclins A, B and B3 in *Drosophila* female meiosis. G3 Genes Genom Genet 6, 3711–3724.
Burke, B. (2012). It takes KASH to hitch to the SUN. Cell 149, 961–963.
Camlin, N.J., McLaughlin, E.A., and Holt, J.E. (2017). Motoring through: the role of kinesin superfamily proteins in female meiosis. Human Reproduction Update 23, 409–420.

Carlton, P.M., Cowan, C.R., and Cande, W.Z. (2003). Directed motion of telomeres in the formation of the meiotic bouquet revealed by time course and simulation analysis. MBoC 14, 2832–2843.
Cassidy-Hanley, D., Bowen, J., Lee, J.H., Cole, E., VerPlank, L.A., Gaertig, J., Gorovsky, M.A., and Bruns, P.J. (1997). Germline and somatic transformation of mating *Tetrahymena thermophila* by particle bombardment. Genetics 146, 135–147.
Cervantes, M.D., Xi, X., Vermaak, D., Yao, M.C., and Malik, H.S. (2006). The CNA1 Histone of the ciliate*Tetrahymena thermophila* is dssential for chromosome segregation in the germline micronucleus. MBoC 17, 485–497.
Chen, X., Gao, S., Liu, Y., Wang, Y., Wang, Y., and Song, W. (2016). Enzymatic and chemical mapping of nucleosome distribution in purified micro- and macronuclei of the ciliated model organism, *Tetrahymena thermophila*. Sci China Life Sci 59, 909–919.
Collins, K., and Gorovsky, M.A. (2005). *Tetrahymena thermophila*. Curr Biol 15, R317–R318.
Cui, B., and Gorovsky, M.A. (2006). Centromeric histone H3 is essential for vegetative cell division and for DNA elimination during conjugation in *Tetrahymena thermophila*. Mol Cell Biol 26, 4499–4510.
Eisen, J.A., Coyne, R.S., Wu, M., Wu, D., Thiagarajan, M., Wortman, J.R., Badger, J.H., Ren, Q., Amedeo, P., Jones, K.M., et al. (2006). Macronuclear genome sequence of the ciliate *Tetrahymena thermophila*, a model eukaryote. PLoS Biol 4, e286.
Galderisi, U., Jori, F.P., and Giordano, A. (2003). Cell cycle regulation and neural differentiation. Oncogene 22, 5208–5219.
Gallant, P., and Nigg, E.A. (1994). Identification of a novel vertebrate cyclin: cyclin B3 shares properties with both A- and B-type cyclins.. EMBO J 13, 595–605.
Gao, S., Xiong, J., Zhang, C., Berquist, B.R., Yang, R., Zhao, M., Molascon, A.J., Kwiatkowski, S.Y., Yuan, D., Qin, Z., et al. (2013). Impaired replication elongation in *Tetrahymena* mutants deficient in histone H3 Lys 27 monomethylation. Genes Dev 27, 1662–1679.
Gautier, J., and Maller, J.L. (1991). Cyclin B in Xenopus oocytes: implications for the mechanism of pre-MPF activation.. EMBO J 10, 177–182.
Ghosh, S., and Chan, C. (2016). Analysis of RNA-seq data using TopHat and Cufflinks. Methods Mol Biol 1374, 339–361.
Golczyk, H., Musiał, K., Rauwolf, U., Meurer, J., Herrmann, R.G., and Greiner, S. (2008). Meiotic events in *Oenothera*—a non-standard pattern of chromosome behaviour. Genome 51, 952–958.
Gorovsky, M.A., Yao, M.C., Keevert, J.B., and Pleger, G.L. (1975). Isolation of micro-and macronuclei of *Tetrahymena pyriformis*. Methods Cell Biol 9, 311–327.
Grelon, M., Vezon, D., Gendrot, G., and Pelletier, G (2001). AtSPO11-1 is necessary for efficient meiotic recombination in plants. EMBO J 20, 589–600.
Hagting, A., Karlsson, C., Clute, P., Jackman, M., and Pines, J. (1998). MPF localization is controlled by nuclear export. EMBO J 17, 4127–4138.
Hayashi, A., and Mochizuki, K. (2015). Targeted gene disruption by ectopic induction of DNA elimination in *Tetrahymena*. Genetics 201, 55–64.
Howard-Till, R.A., Lukaszewicz, A., and Loidl, J. (2011). The recombinases Rad51 and Dmc1 play distinct roles in DNA break repair and recombination partner choice in the meiosis of *Tetrahymena*. PLoS Genet 7, e1001359.
Huysman, M.J.J., Martens, C., Vandepoele, K., Gillard, J., Rayko, E., Heijde, M., Bowler, C., Inzé, D., Van de Peer, Y., De Veylder, L., et al. (2010). Genome-wide analysis of the diatom cell cycle unveils a novel type of cyclins involved in environmental signaling. Genome Biol 11, R17.
Kushida, Y., Takaine, M., Nakano, K., Sugai, T., Vasudevan, K.K., Guha, M., Jiang, Y.Y., Gaertig, J., and Numata, O. (2017). Kinesin-14 is important for chromosome segregation during mitosis and meiosis in the ciliate *Tetrahymena thermophila*. J Eukaryot Microbiol 64, 293–307.
Lindqvist, A., Rodríguez-Bravo, V., and Medema, R.H. (2009). The decision to enter mitosis: feedback and redundancy in the mitotic entry network. J Cell Biol 185, 193–202.
Loidl, J., Lukaszewicz, A., Howard-Till, R.A., and Koestler, T. (2012). The *Tetrahymena* meiotic chromosome bouquet is organized by centromeres and promotes interhomolog recombination. J Cell Sci 125, 5873–5880.
Loidl, J., and Mochizuki, K. (2009). *Tetrahymena* meiotic nuclear reorganization is induced by a checkpoint kinase–dependent response to DNA damage. Mol Biol Cell 20, 2428–2437.
Loidl, J., and Scherthan, H. (2004). Organization and pairing of meiotic chromosomes in the ciliate *Tetrahymena thermophila*. J Cell Sci 117, 5791–5801.
Müller-Tidow, C., Ji, P., Diederichs, S., Potratz, J., Bäumer, N., Köhler, G., Cauvet, T., Choudary, C., van der Meer, T., Chan, W.Y.I., et al. (2004). The cyclin A1-CDK2 complex regulates DNA double-strand break repair. Mol Cellular Biol 24, 8917–8928.
Magnard, J.L., Yang, M., Chen, Y.C.S., Leary, M., and McCormick, S. (2001). The Arabidopsis gene *tardy asynchronous meiosis* is required for the normal pace and synchrony of cell division during male meiosis. Plant Physiol 127, 1157–1166.
Martindale, D., Allis, C., and Bruns, P. (1982). Conjugation in Tetrahymena thermophila: a temporal analysis of cytological stages. Exp Cell Res 140, 227–236.
Martindale, D.W., Allis, C.D., and Bruns, P.J. (1985). RNA and protein synthesis during meiotic prophase in *Tetrahymena thermophila*. J Protozool 32, 644–649.
Mochizuki, K. (2008). High efficiency transformation of *Tetrahymena* using a codon-optimized neomycin resistance gene. Gene 425, 79–83.
Mochizuki, K., and Gorovsky, M.A. (2005). A Dicer-like protein in *Tetrahymena* has distinct functions in genome rearrangement, chromosome segregation, and meiotic prophase. Genes Dev 19, 77–89.
Mochizuki, K., Novatchkova, M., and Loidl, J. (2008). DNA double-strand breaks, but not crossovers, are required for the reorganization of meiotic nuclei in *Tetrahymena*. J Cell Sci 121, 2148–2158.
Morgan, D.O. (1997). Cyclin-dependent kinases: engines, clocks, and microprocessors. Annu Rev Cell Dev Biol 13, 261–291.
Nguyen, T.B., Manova, K., Capodieci, P., Lindon, C., Bottega, S., Wang, X. Y., Refik-Rogers, J., Pines, J., Wolgemuth, D.J., and Koff, A. (2002). Characterization and expression of mammalian cyclin b3, a prepachytene meiotic cyclin. J Biol Chem 277, 41960–41969.
Niccoli, T., Yamashita, A., Nurse, P., and Yamamoto, M. (2004). The p150-Glued Ssm4p regulates microtubular dynamics and nuclear movement in fission yeast. J Cell Sci 117, 5543–5556.
Nieduszynski, C.A., Murray, J., and Carrington, M. (2002). Whole-genome analysis of animal A-and B-type cyclins. Genome Biol 3, research0070.1.
Noto, T., and Mochizuki, K. (2017). Whats, hows and whys of programmed DNA elimination in *Tetrahymena*. Open Biol 7, 170172.
Orias, E., Cervantes, M.D., and Hamilton, E.P. (2011). *Tetrahymena thermophila*, a unicellular eukaryote with separate germline and somatic genomes. Res Microbiol 162, 578–586.
Orias, E., and Flacks, M. (1975). Macronuclear genetics of *Tetrahymena* I. Random distribution of macronuclear gene copies in *T. pyriformis*, syngen 1. Genetics 79, 187–206.
Ozaki, Y., Saito, K., Shinya, M., Kawasaki, T., and Sakai, N. (2011). Evaluation of Sycp3, Plzf and Cyclin B3 expression and suitability as spermatogonia and spermatocyte markers in zebrafish. Gene Expression Patterns 11, 309–315.
Papazyan, R., Voronina, E., Chapman, J.R., Luperchio, T.R., Gilbert, T.M., Meier, E., Mackintosh, S.G., Shabanowitz, J., Tackett, A.J., Reddy, K. L., et al. (2014). Methylation of histone H3K23 blocks DNA damage in pericentric heterochromatin during meiosis. eLife 3, e02996.
Pines, J., and Hunter, T. (1994). The differential localization of human cyclins A and B is due to a cytoplasmic retention signal in cyclin B.. EMBO J 13, 3772–3781.
Smith, K.N., Penkner, A., Ohta, K., Klein, F., and Nicolas, A. (2001). B-type cyclins *CLB5* and *CLB6* control the initiation of recombination and

synaptonemal complex formation in yeast meiosis. Curr Biol 11, 88–97.
Stover, N.A., Krieger, C.J., Binkley, G., Dong, Q., Fisk, D.G., Nash, R., Sethuraman, A., Weng, S., and Cherry, J.M. (2006). *Tetrahymena* Genome Database (TGD): a new genomic resource for *Tetrahymena thermophila* research. Nucl Acids Res 34, D500–D503.
Stover, N.A., and Rice, J.D. (2011). Distinct cyclin genes define each stage of ciliate conjugation. Cell Cycle 10, 1699–1701.
Sugai, T., and Hiwatashi, K. (1974). Cytologic and autoradiographic studies of the micronucleus at meiotic prophase in *Tetrahymena pyriformis*. J Protozoology 21, 542–548.
Trelles-Sticken, E., Bonfils, S., Sollier, J., Géli, V., Scherthan, H., and de La Roche Saint-André, C. (2005). Set1- and Clb5-deficiencies disclose the differential regulation of centromere and telomere dynamics in Saccharomyces cerevisiae meiosis. J Cell Sci 118, 4985–4994.
Trelles-Sticken, E., Loidl, J., and Scherthan, H. (1999). Bouquet formation in budding yeast: initiation of recombination is not required for meiotic telomere clustering. J Cell Sci 112, 651–658.
Tschöp, K., Müller, G.A., Grosche, J., and Engeland, K. (2006). Human cyclin B3. mRNA expression during the cell cycle and identification of three novel nonclassical nuclear localization signals. FEBS J 273, 1681–1695.
Wang, Y.R., Wang, Y., Sheng, Y., Huang, J., Chen, X., Al-Rasheid, K.A.S., and Gao, S. (2017). A comparative study of genome organization and epigenetic mechanisms in model ciliates, with an emphasis on *Tetrahymena , Paramecium* and *Oxytricha*. Eur J Protistol 61, 376–387.
Wang, Y.Y., Chen, X., Sheng, Y., Liu, Y., and Gao, S. (2017a). N^6-adenine DNA methylation is associated with the linker DNA of H2A.Z-containing well-positioned nucleosomes in Pol II-transcribed genes in *Tetrahymena*. Nucl Acids Res 45, 11594–11606.
Wang, Y.Y., Sheng, Y., Liu, Y., Pan, B., Huang, J., Warren, A., and Gao, S. (2017b). N^6-methyladenine DNA modification in the unicellular eukaryotic organism Tetrahymena thermophila. Eur J Protistol 58, 94–102.
Woglar, A., and Jantsch, V. (2014). Chromosome movement in meiosis I prophase of *Caenorhabditis elegans*. Chromosoma 123, 15–24.
Wolfe, J. (1973). Conjugation in *Tetrahymena*: the relationship between the division cycle and cell pairing. Dev Biol 35, 221–231.
Woo, T.T., Chao, J.L., and Yao, M.C. (2016). Dynamic distributions of long double-stranded RNA in *Tetrahymena* during nuclear development and genome rearrangements. J Cell Sci 129, 1046–1058.
Xiong, J., Lu, Y., Feng, J., Yuan, D., Tian, M., Chang, Y., Fu, C., Wang, G., Zeng, H., and Miao, W. (2013). *Tetrahymena* functional genomics database (TetraFGD): an integrated resource for *Tetrahymena* functional genomics. Database 2013, bat008.
Xu, J., Tian, H., Wang, W., and Liang, A. (2012). The zinc finger protein Zfr1p is localized specifically to conjugation junction and required for sexual development in *Tetrahymena thermophila*. PLoS ONE 7, e52799.
Xu, Q., Wang, R., Ghanam, A.R., Yan, G., Miao, W., and Song, X. (2016). The key role of *CYC2* during meiosis in *Tetrahymena thermophila*. Protein Cell 7, 236–249.
Yan, G.X., Dang, H., Tian, M., Zhang, J., Shodhan, A., Ning, Y.Z., Xiong, J., and Miao, W. (2016a). Cyc17, a meiosis-specific cyclin, is essential for anaphase initiation and chromosome segregation in *Tetrahymena thermophila*. Cell Cycle 15, 1855–1864.
Yan, G.X., Zhang, J., Shodhan, A., Tian, M., and Miao, W. (2016b). Cdk3, a conjugation-specific cyclin-dependent kinase, is essential for the initiation of meiosis in *Tetrahymena thermophila*. Cell Cycle 15, 2506–2514.
Zhang, T., Qi, S.T., Huang, L., Ma, X.S., Ouyang, Y.C., Hou, Y., Shen, W., Schatten, H., and Sun, Q.Y. (2015). Cyclin B3 controls anaphase onset independent of spindle assembly checkpoint in meiotic oocytes. Cell Cycle 14, 2648–2654.
Zhao, X., Wang, Y., Wang, Y., Liu, Y., and Gao, S. (2017). Histone methyltransferase TXR1 is required for both H3 and H3.3 lysine 27 methylation in the well-known ciliated protist Tetrahymena thermophila. Sci China Life Sci 60, 264–270.
Zickler, D., and Kleckner, N. (2016). A few of our favorite things: Pairing, the bouquet, crossover interference and evolution of meiosis. Seminars Cell Dev Biol 54, 135–148.

SUPPORTING INFORMATION

Figure S1 Characterization of Cyc2p.

Figure S2 Generation of OE-CYC2 and CRS-CYC2 mutant strains.

Figure S3 Relative fluorescence intensity of Mics. The relative fluorescence intensity of micronuclei (n=10) was measured using MetaMorph 7.8.13 software. The black points indicate the median; the black rhombuses indicate the max or min values.

Table S1 Primers used in mutant strain construction

The supporting information is available online at http://life.scichina.com and https://link.springer.com. The supporting materials are published as submitted, without typesetting or editing. The responsibility for scientific accuracy and content remains entirely with the authors.